Impact of Equivalence Ratio on the Macrostructure of Premixed Swirling CH[subscript 4]/Air and CH[subscript 4]/O[subscript 2]/CO[subscript 2] Flames

Proceedings of ASME Turbo Expo 2015: Turbine Technical Conference and Exposition
GT2015
June 15 – 19, 2015, Montréal, Canada

GT2015-43224

IMPACT OF EQUIVALENCE RATIO ON THE MACROSTRUCTURE OF PREMIXED SWIRLING CH_4/AIR AND $CH_4/O_2/CO_2$ FLAMES

Hirotatsu Watanabe
Massachusetts Institute of Technology
Cambridge, Massachusetts, USA

Santosh J. Shanbhogue
Massachusetts Institute of Technology
Cambridge, Massachusetts, USA

Ahmed F. Ghoniem
Massachusetts Institute of Technology
Cambridge, Massachusetts, USA

ABSTRACT

Premixed $CH_4/O_2/CO_2$ flames (oxy-flames) and CH_4/air flames (air-flames) were experimentally studied in a swirl-stabilized combustor. For comparing oxy and air flames, the same equivalence ratio and adiabatic flame temperature were used. CO_2 dilution was adjusted to attain the same adiabatic temperature for the oxy-flame and the corresponding air-flame while keeping the equivalence ratio and Reynolds number (=20,000) the same. For high equivalence ratios, we observed flames stabilized along the inner and outer shear layers of the swirling flow and sudden expansion, respectively, in both flames. However, one notable difference between the two flames appears as the equivalence ratio reaches 0.60. At this point, the outer shear layer flame disappears in the air-flame while it persists in the oxy-flame, despite the lower burning velocity of the oxy-flame. Prior PIV measurements (Ref. 9) showed that the strains along the outer shear layer are higher than along the inner shear layer. Therefore, the extinction strain rates in both flames were calculated using a counter-flow premixed twin flame configuration. Calculations at the equivalence ratio of 0.60 show that the extinction strain rate is higher in the oxy than in the air flame, which help explain why it persists on the outer shear layer with higher strain rate. It is likely that extinction strain rates contribute to the oxy-flame stabilization when air flame extinguish in the outer shear layer. However, the trend reverses at higher equivalence ratio, and the cross point of the extinction strain rate appears at equivalence ratio of 0.64.

INTRODUCTION

Carbon dioxide has attracted attention as a greenhouse gas, that contributes to global warming. Carbon Capture and Storage (CCS) technologies have gained interest because they may have the potential to reduce CO_2 emissions. Oxy-fuel combustion is a promising technology for CO_2 capture [1]. It has some advantages such as lower NO_x emission and lower energy penalty with CO_2 removal [2,3]. The substitution of N_2 with CO_2 as a diluent alters the flame characteristics. For instance, the laminar burning velocity in O_2/CO_2 mixtures is much lower than that in air because of its impact on the specific heat and transport properties. Moreover, CO_2 is not inert but participates in the chemical reactions. The successful implementation of oxy-fuel combustion in gas turbines depends on gaining better understanding of the differences that result from the replacement of N_2 with CO_2. The effect of CO_2 dilution on flame characteristics has been extensively studied recently using Bunsen-type turbulent premixed flames [4], counterflow non-premixed flame [5], and swirl-stabilized-flames [6]. Knowledge of the flame structure at the macro and microscales and their relation to dynamics and stability are essential for the safe operations of these systems. Studying the dynamics and stability in premixed $CH_4/O_2/CO_2$ flames is also important to achieve compact flames with lower CO and soot emissions. Recently, Shroll *et al.* studied dynamic stability characteristics of premixed $CH_4/O_2/CO_2$ mixtures in the MIT swirl stabilized combustor, and found that the transition between instability modes correlated with the adiabatic flame temperature [6]. Further work in the same group [7,8] showed that the correlation between the flame structure and the dynamic mode, with flames stabilized on the inner shear layer around the inner recirculation zone being stable while flames stabilized in the inner shear layer as well as the outer shear layer being unstable.

In this paper, premixed CH_4/air flames (air-flames) and $CH_4/O_2/CO_2$ flames (oxy-flames) under stable conditions (in the absence of thermoacoustic instabilities) are experimentally examined in the same combustor using OH-PLIF. Moreover, flame extinction strains are computed in the twin flame configuration to explain some of the trends in the experiment.

EXPERIMENT

Figure 1 and Figure 2 show a confined premixed-swirl stabilized combustor with a sudden expansion similar to those found in modern gas turbines. A premixed flame is stabilized using a combination of swirl and sudden expansion. The experimental setup has been described in detail in our previous publications [6-10]. Premixed $CH_4/O_2/CO_2$ or premixed CH_4/air enters the combustor through a 38 mm diameter inlet pipe. The swirler is located 52.3 mm upstream of the expansion plane and has 8 blades with an estimated swirl number of 0.53 [6]. Flow expands into a 400 mm length, and 76 mm diameter combustion chamber (Fig. 2), and the test section is equipped with a quartz tube for optical access. Air, CO_2, O_2, and CH_4 are each supplied using Sierra Instruments mass flow controllers. The accuracy of each is $\pm$ 2 % of full scale. Inlet pressure and temperature are atmospheric and room temperature, respectively.

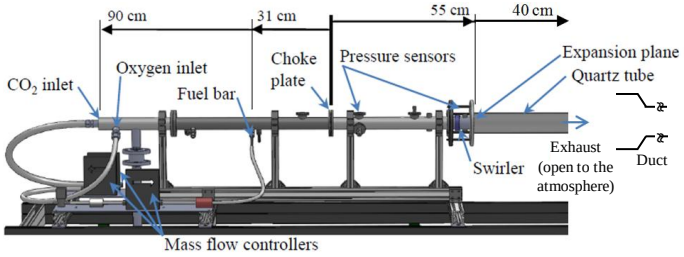

Figure 1 : Overview of axisymetric swirl combustor

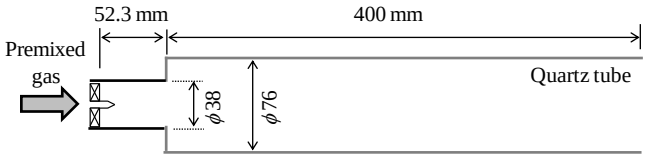

Figure 2 : Details of swirl combustor

A useful reference for comparing oxy-flames with air-flames is the adiabatic flame temperature. The same equivalence ratio and adiabatic flame temperature were used for appropriate comparison of the flame structure between the air and oxy-flames in this study, (although for practical systems near-stoichiometric conditions are desired for the latter to avoid any excess oxygen in the combustion products [6]). CO_2 dilution was adjusted to attain the same adiabatic temperature for oxy-flames and the corresponding air-flames while keeping the equivalence ratio and Reynolds number (=20,000) the same. The equivalence ratio (ϕ) was set to 0.60 and 0.65 in both air and oxy-flames. Details will be described later.

Flame photographs were taken using a digital camera (Nikon D5100). These were used to describe the time-averaged flame shape, what we also refer to as the 'macrostructure'. Planar laser-induced fluorescence (PLIF) measurement of OH radicals was used to examine the flame shape. OH-LIF signals were measured by exciting the Q1(8) line of the $A^2\Sigma\,(v'=1) \leftarrow X^2\Sigma\,(v''=0)$ transition band of OH at 283.56 nm. This was accomplished using a 220 mJ/pulse, 355 nm Nd:YAG pump beam from a Spectra-Physics LAB-170 laser routed in a Sirah Cobrastretch dye laser circulating Coumarin 153 dye dissolved in ethanol. The resonator in the dye laser converts this beam to 567 nm which is then frequency-doubled using a BBO crystal and compensator to 283.56 nm beam with approximately 13 mJ/pulse. This beam is then expanded into a sheet using a combination of cylindrical (-50mm) and spherical lenses (-75mm and +85mm). Emission was collected by 640 x 512 pixel LaVision Nanostar CCD camera with a 308 $\pm$ 10 nm optical filter. A f/2.8 Cerco UV-lens was used to focus the PLIF emission from the combustor onto the camera. The camera was not flat-fielded. The images were recorded at 10 Hz with a gating time of 100 ns. Images were post-processed by normalizing the intensities in each image with the maximum intensities of the brightness. In addition to average flame configuration and OH-PLIF images, high-speed chemiluminescence images were taken at 500 fps using a NAC GX-1 high-speed CMOS camera with a Nikon 50 mm f/1.8 lens. The camera has a resolution of 1280 x 1024 pixel and a monochrome bit depth of 12 bits per pixel. Schott BG-39 optical colored glass filter with 2 mm thickness is placed in front of camera to attenuate infrared radiation from the flame.

Figure 3 (a) and (b) show the chemiluminescence images of the air flame at ϕ = 0.65 and schematic diagram of its flow pattern in the swirl-stabilized combustor. Many researchers have studied flow patterns in swirl stabilized combustor [11-13]. The flow pattern consists of several regions: The outer recirculation zone (ORZ), created by the sudden expansion of the nozzle; the inner recirculation zone (IRZ), created by the adverse pressure gradient caused by the swirl motion; and the reactants jet between the two zones confined by the inner and outer shear layers.

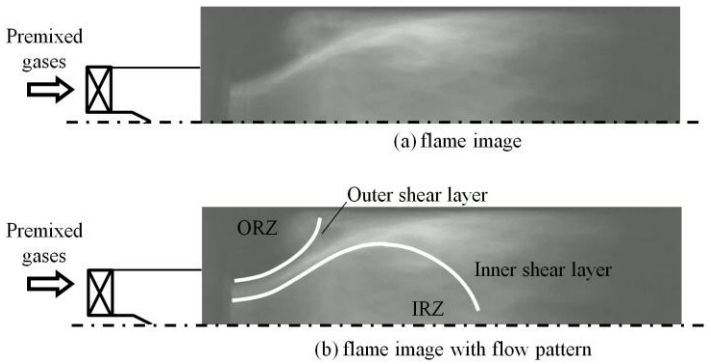

Figure 3 : Chemiluminescence image of (a) air flame at ϕ = 0.65 and (b) schematic diagram of its flow patterns

COMPUTATION

Flame extinction was numerically examined in premixed twin flame configuration shown in Figure 4. Twin flames are formed near the stagnation plane of the two opposed CH_4/Air or $CH_4/O_2/CO_2$ flows. In this study, the distance between two nozzles is fixed at 1.4 cm for all calculations. The conservation equations for steady quasi one-dimensional premixed flames were solved using CHEMKIN-PRO. The extinction strain rate is obtained from the response of the maximum temperature to the strain rate in the twin premixed flame configuration. The air-flame ($CH_4/O_2/N_2$) was modeled using GRI-Mech 3.0. It involved 53 species and 325

elementary reactions. For the oxy-flame ($CH_4/O_2/CO_2$), the reaction mechanism proposed by Mendiara and Glarborg [14], from which nitrogen chemistry was removed, was used. This mechanism was verified for oxy-flames. It involves 49 species and 350 elementary reactions. In this calculation, radiation is not considered.

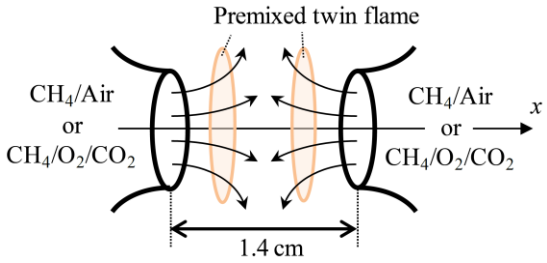

Figure 4 : Schematic diagram of the premixed twin flame configuration

Table 1 shows the adiabatic flame temperature (T_{ad}) and laminar flame velocity (S_L) at the experimental conditions. The inlet O_2 mole fraction in oxidizer flow (X'_{O2}) and inlet CO_2 mole fraction in reactant flow (X_{CO2}) are defined as follows:

$$X'_{O_2} = \frac{Q_{O_2,\text{inlet}}}{Q_{O_2,\text{inlet}} + Q_{N_2,\text{inlet}}} \quad \text{(for air-flames)} \qquad (1)$$

$$X'_{O_2} = \frac{Q_{O_2,\text{inlet}}}{Q_{O_2,\text{inlet}} + Q_{CO_2,\text{inlet}}} \quad \text{(for oxy-flames)} \qquad (2)$$

$$X_{CO_2} = \frac{Q_{CO_2,\text{inlet}}}{Q_{CH_4,\text{inlet}} + Q_{O_2,\text{inlet}} + Q_{CO_2,\text{inlet}}} \quad \text{(for oxy-flames)} \qquad (3)$$

where $Q_{i,\text{inlet}}$ indicates the volume gas flow rate of species i.

The adiabatic temperatures of the oxy-flames were almost the same as those of the air-flames at the same ϕ, whereas the laminar burning velocities of oxy-flames were consistently lower than those of the air-flames. All cases were calculated at atmospheric pressure, and the inlet reactant temperature was 300 K.

Table 1: Experimental conditions (*Re* = 20,000)

ϕ = 0.65 [-]	X'_{O2} [-]	X_{CO2} [-]	T_{ad} [K]	S_L [cm s^{-1}]
Air	0.21	-	1752	15.3
Oxy	0.30	0.637	1754	9.53
ϕ = 0.62 [-]	X'_{O2} [-]	X_{CO2} [-]	T_{ad} [K]	S_L [cm s^{-1}]
Air	0.21	-	1700	12.9
Oxy	0.30	0.640	1701	8.13
ϕ = 0.60 [-]	X'_{O2} [-]	X_{CO2} [-]	T_{ad} [K]	S_L [cm s^{-1}]
Air	0.21	-	1666	11.4
Oxy	0.30	0.642	1667	7.23

RESULTS AND DISCUSSION

Time-Averaged Flame Shapes/Macrostructures

Figure 5 shows the average flame shapes of air and oxy-flames at various equivalence ratios.

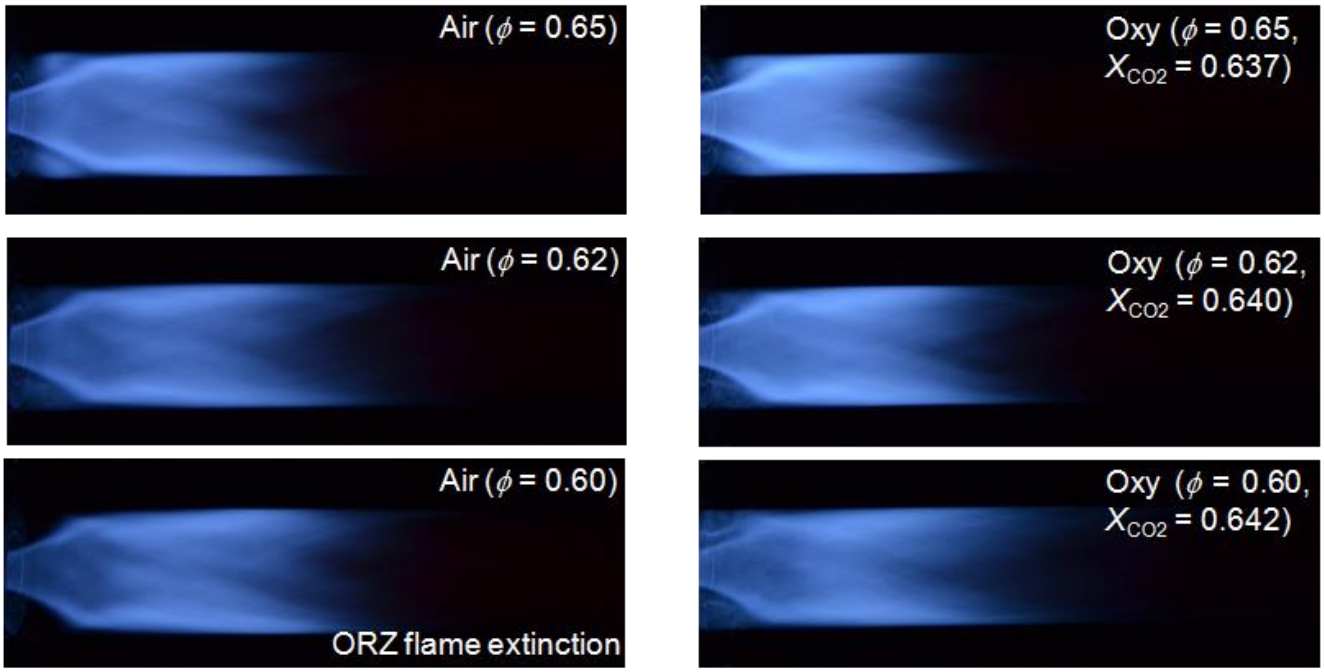

Figure 5 : Mean flame shapes of air and oxy-flame at various equivalence ratios

In our previous work [7-10], we analyzed premixed air flames in the swirl-stabilized combustor, and observed four different shapes/configurations that appear as the equivalence ratio is raised or the laminar burning velocity of the corresponding flame increases: columnar flame (I); a bubble+columnar flame (II); a single conical flame (III); and a double conical flame (IV). In flame III (e.g. as seen in Figure 5 bottom-left), the flame is stabilized along the inner shear layer, while in flame IV (e.g. as seen in Figure 5, bottom-right), it is stabilized along both the inner and outer shear layers. In this study, configuration IV -- where the flame appears in outer shear layer -- is found in most of air and oxy-flames except for air flame at $\phi = 0.60$.

Overall, as the equivalence ratio is reduced, the flame length becomes longer in both cases. The key difference between the two flames appears as the equivalence ratio reaches 0.60, when the outer shear layer flame disappears in the air-flame while it persists in the oxy-flame (see Figure 5, last row). Configuration III, where the flame is stabilized on the inner shear layer only is found in the air-flame at $\phi = 0.60$, whereas configuration IV is found in the oxy-flame at the same equivalence ratio. This is surprising since the laminar burning velocity of the air flame is higher than the oxy flame as shown in Table 1, and hence it should have been expected to be present in the air-flame according to the dependence of the flame configuration on the burning velocity [7-10]. Meanwhile, when the equivalence ratio is below 0.58, the flame length significantly increases, and a conical flame (configuration III) appears in both air and oxy-flames. Flame stabilization in the outer shear layer which occurs earlier (as the equivalence ratio is raised) in the oxy-flame than in the air-flame is of particular interest in this study.

OH-PLIF images

Figure 6 shows the instantaneous OH-PLIF images for air and oxy-flames near the expansion section at equivalence ratio of 0.65. A wrinkled flame front can be recognized in both OH-PLIF images, appearing in the inner and outer shear layers. Insignificant difference is observed in the flame structures between air and oxy-flames at $\phi = 0.65$.

Figure 7 shows the macrostructure and instantaneous OH-PLIF images for air and oxy-flames near the expansion section at $\phi = 0.60$. As seen in Figure 7, the flame fronts are similarly wrinkled; however, an important finding here is that a flame is not stabilized in the outer shear layer in the air flame, whereas it is still stabilized in the oxy-flame as shown in OH-PLIF images (Figure 7(b)). In the following we attempt to explain this observation using flame extinction based arguments. We note that other mechanism may also contribute to this observation [15]

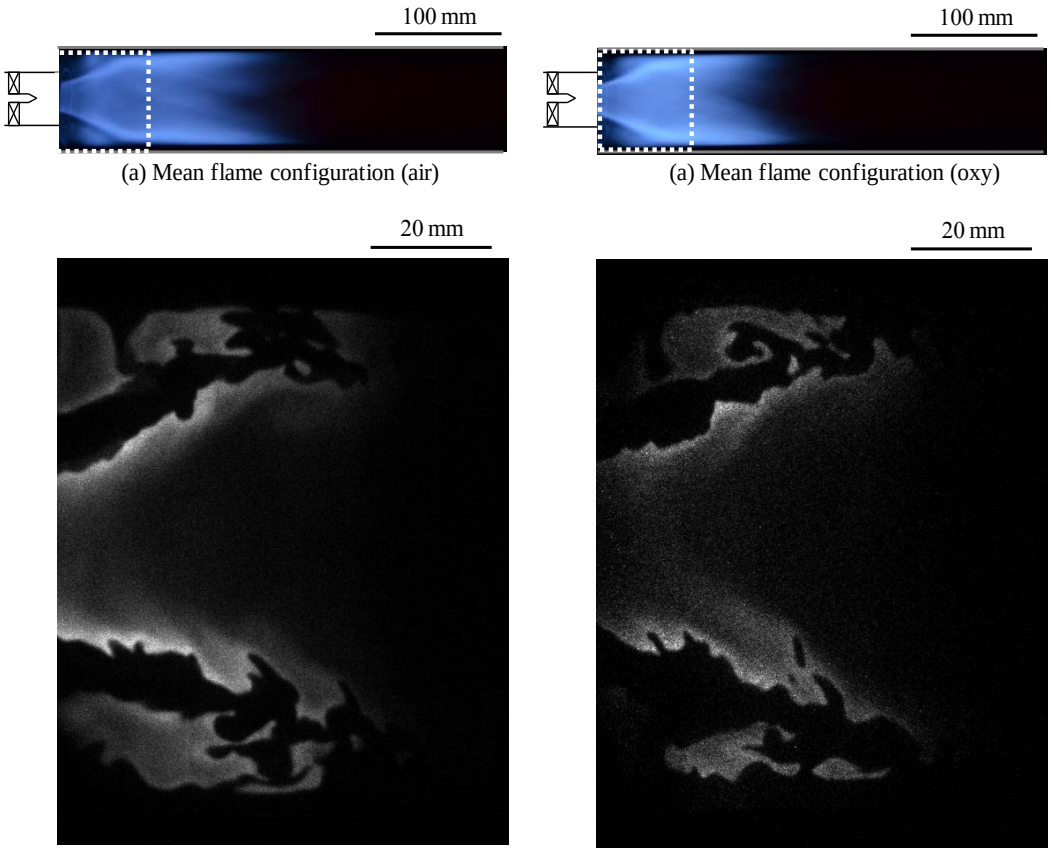

(a) Mean flame configuration (air)

(a) Mean flame configuration (oxy)

(b) OH-PLIF (air, $\phi = 0.65$)

(b) OH-PLIF (oxy, $\phi = 0.65$)

Figure 6 : Mean flame configuration and OH-PLIF images near inlet nozzle of air and oxy-flames at $\phi = 0.65$

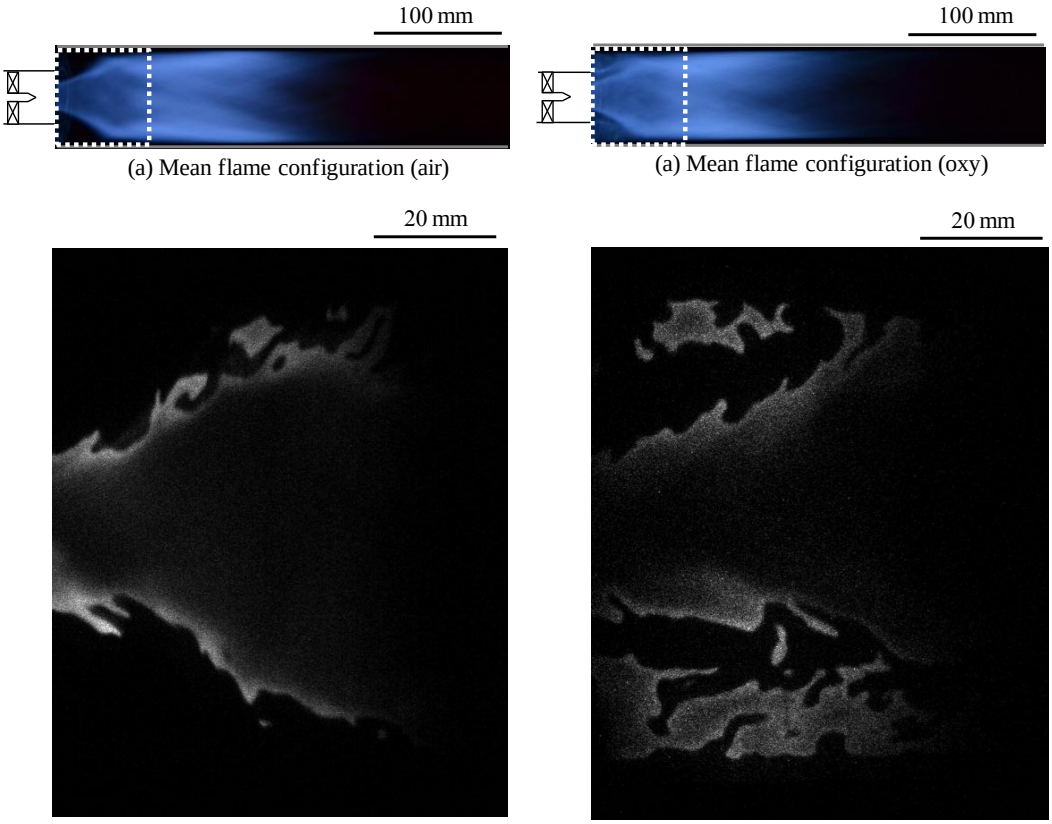

(a) Mean flame configuration (air)

(a) Mean flame configuration (oxy)

(b) OH-PLIF (air, $\phi = 0.60$)

(b) OH-PLIF (oxy , $\phi = 0.60$)

Figure 7 : Mean flame configuration and OH-PLIF images near inlet nozzle of air and oxy-flames at $\phi = 0.60$

Mean OH-PLIF images and strain rate

Figure 8 shows the mean OH-PLIF images for air and oxy-flames at ϕ = 0.60. 128 OH-PLIF images were used in averaging procedure. Previously, LaBry *et al*. performed PIV measurements on CH_4/air flame in the same swirl-stabilized combustor, and estimated the two dimensional strain rate shown in Figure 9 [9]. Figure 9 shows mean flow structures where the flame is stabilized along the inner shear layer (ϕ = 0.60, (a)) or it is stabilized along both the inner and outer shear layer (ϕ = 0.65, (b)). Details are shown in elsewhere [9].

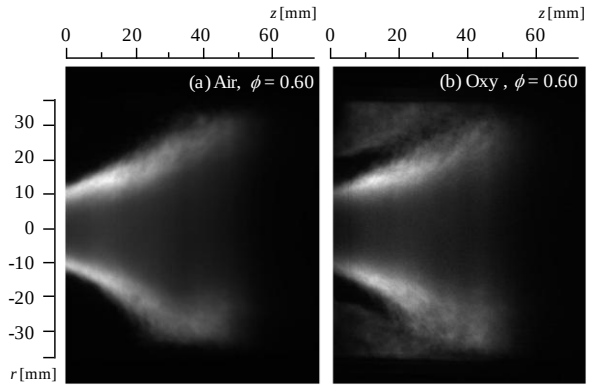

Figure 8 : Mean OH-PLIF images near inlet nozzle of air (left) and oxy-flames (right) at $\phi = 0.60$

Strain rates along the outer shear layer are higher than those along the inner shear layer in both cases.

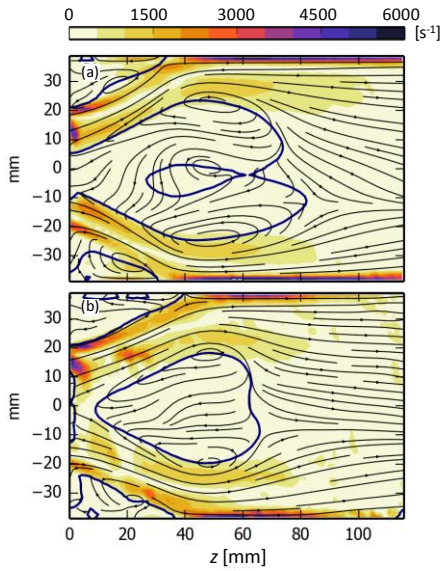

Figure 9 : Mean flow structures at $\phi = 0.60$ (Flame III, (a)) and $\phi = 0.65$ (Flame IV, (b)). Streamlines indicate the mean flow direction and contours show the mean location of zero axial velocity. Shading indicates the magnitude of the strain rate (CH_4/air flame, *Re* = 20,000) [9].

By using mean OH-PLIF images (Figure 8) and strain rates (Figure 9(a)) at ϕ = 0.60, OH intensity and strain rate profiles are produced. Figure 10 shows profiles of normalized OH intensity (mean OH intensity normalized by its maximum value) and strain rate at z = 5, 15, and 25 mm.

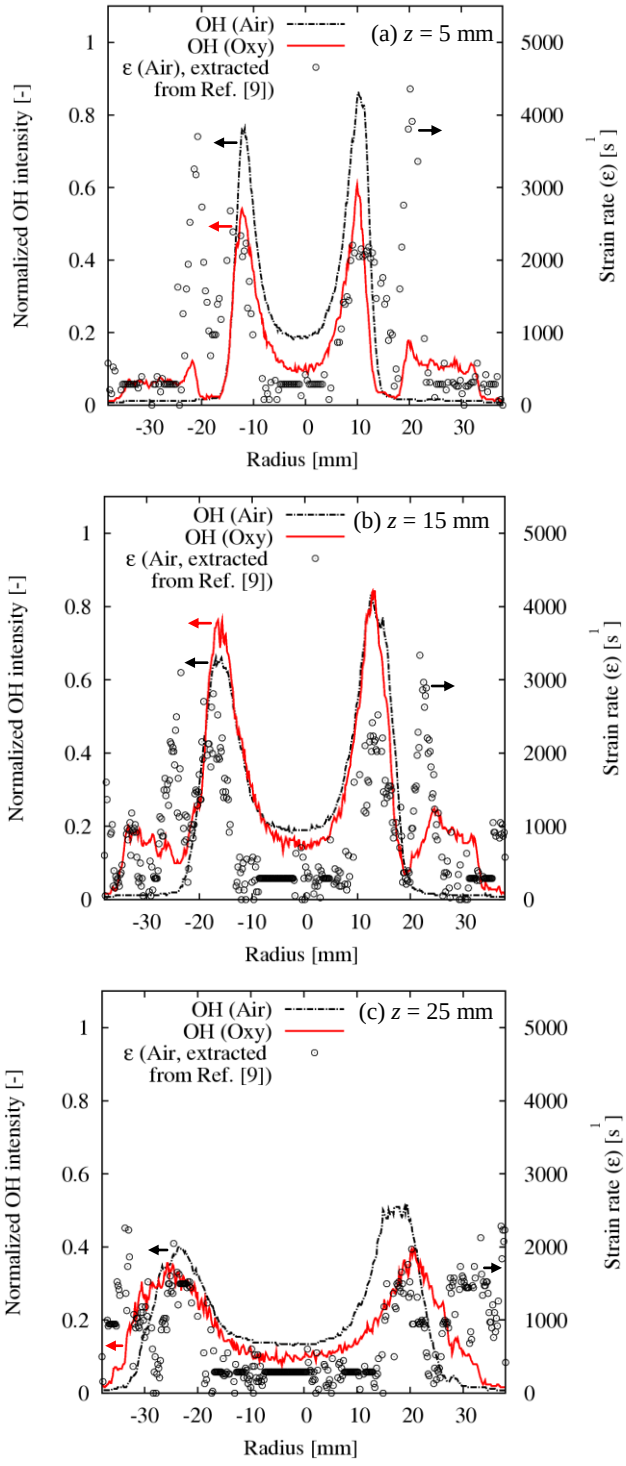

Figure 10 : Normalized OH intensity and strain rate at ϕ = 0.60

There are four notable peaks in the strain rate profiles. The outer and inner peaks are found at around r = ±20 mm and r = ±10 mm in Figure 10(a), r = ±25 mm and r = ±15 mm in Figure 10(b), and r = ±35 mm and r = ±25 mm in Figure 10(c). These peaks indicate the outer and inner shear layers, respectively. Peaks are also found near wall boundary. At z = 5 mm the strain rates in the outer shear layer are significantly higher than those in the inner shear layer. They are still higher at z = 15 mm but by a smaller margin. Then, they become similar at z = 25 mm. OH signals appear in both air and oxy-flames; however, in the outer shear layer, OH signals do not appear in the air-flames, whereas those appear in the oxy-flames, as described previously. Considering the higher strain rate in the outer shear layer, flame responses to strain might be responsible for oxy-flame stabilization. Air and oxy-flame responses to strains are studied using CHEMKIN in the next section.

Flame extinction calculation

Figure 11 and Figure 12 show the adiabatic flame temperature and the laminar burning velocity for air and oxy-flames at equivalence ratios ranging from 0.60 to 0.68, respectively. When the inlet O_2 mole fraction (X'_{O2}) of the oxidizer is set to 0.30, the adiabatic temperature of oxy-flames is the same as that of air flames and the laminar burning velocity of oxy-flame is lower than that of air-flame in these equivalence ratios.

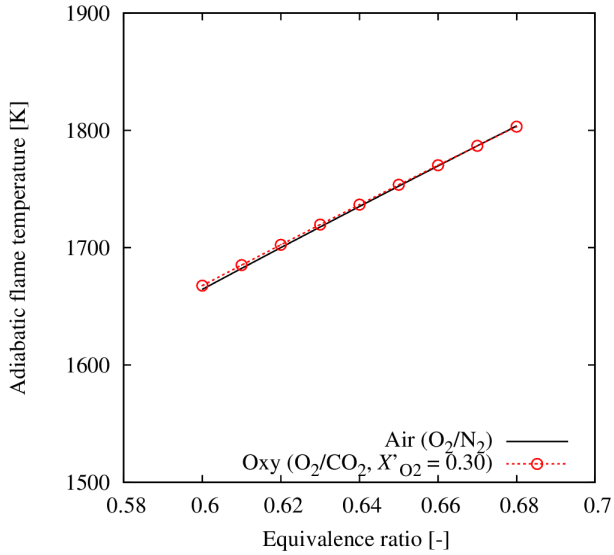

Figure 11 : Adiabatic flame temperature of air and oxy-flames

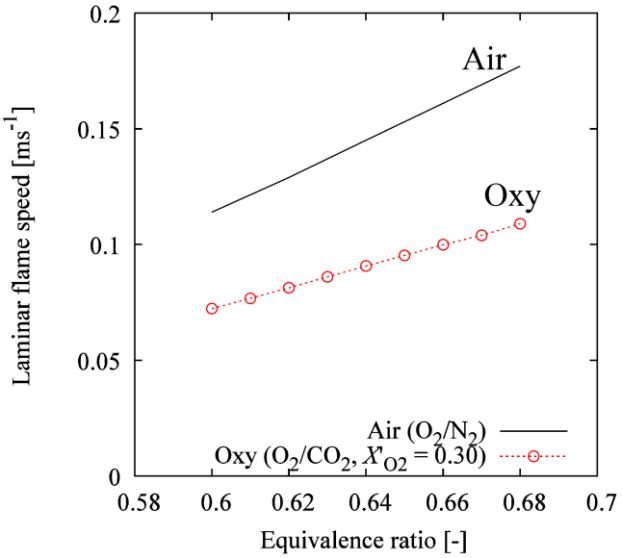

Figure 12: Laminar burning velocity of air and oxy-flames

Figure 13 shows the extinction strain rate of air and oxy-flames at equivalence ratios from 0.60 to 0.68. In air and oxy-flames, the extinction strain rate increases with increasing the equivalence ratio. At low ϕ, the extinction strain rate is higher for oxy-flame, but the opposite is true for higher ϕ. The crossover point appears at ϕ = 0.64. This means that the oxy-flames can survive at higher strains compared to air-flames when equivalence ratio is lower than 0.64, whereas the resistance to extinction of air-flames is higher than oxy-flames when equivalence ratio is higher than 0.64. This may explain why the flame in the outer shear layer disappears in the air-flames while it survives in the oxy-flames at ϕ = 0.6. Furthermore, flames in the outer shear layer are subjected to heat loss because of their proximity to the wall and hence are more vulnerable to extinction earlier than those in the inner shear layer. It is expected that the same trend will be observed as heat loss is taken into consideration; this is currently being investigated. In the next section, we use the numerical results to explain the response of the flame to strain and the mechanisms responsible for raising or lowering the extinction strain for oxy-flames.

Figure 14 shows the response of the flame maximum temperature to strain at ϕ = 0.60 (below the cross point). The adiabatic flame temperature (T_{ad}, 1664 K) is also shown as a dotted line. The maximum flame temperature corresponds to T_{ad} when the strain rate (k) is 0. With increasing the strain rate, first, the maximum temperature increases. This increase is due to the combined effects of the low Lewis number and the positive flame stretch [16]. Since the Lewis number (Le) in the O_2/CO_2 environment is lower than that in the O_2/N_2 environment (Le is 0.76 for O_2/CO_2, and 0.92 for air environments at 300 K), these effects appear more prominently in the oxy-flame. With further increase in the strain rate, the maximum flame temperature starts to decrease, and extinction finally occurs at the turning point. At ϕ = 0.60, the extinction strain rate of the oxy-flame is 545 s^{-1} ($\varepsilon_{ext,oxy}$), whereas it is 495 s^{-1} in air-flames ($\varepsilon_{ext,air}$). This is primarily due to the effect of the transport properties of CO_2.

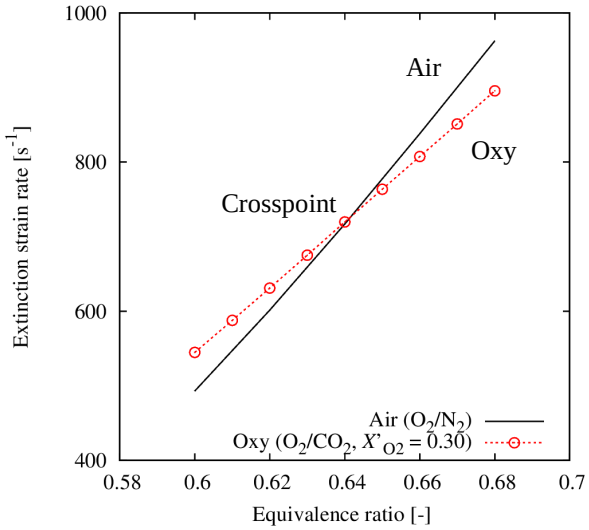

Figure 13: Extinction strain rate of premixed twin air and oxy-flames ($CH_4/O_2/N_2$ vs. $CH_4/O_2/CO_2$)

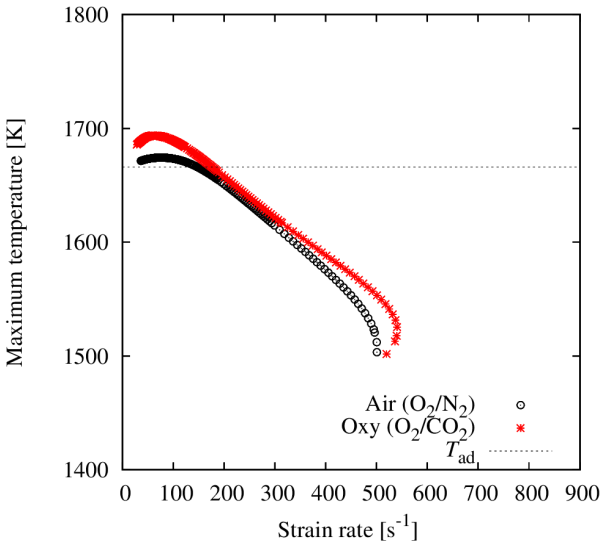

Figure 14 : Response of maximum temperature to the strain rate at ϕ = 0.60

Figure 15 shows the response of the maximum temperature to the strain rate at ϕ = 0.67 (higher than the cross point). The adiabatic flame temperature (T_{ad}, 1787 K) is also shown as a dotted line. Contrary to ϕ = 0.60, the extinction strain rate of oxy-flames ($\varepsilon_{ext,oxy}$ = 837 s^{-1}) is lower than that of air-flames ($\varepsilon_{ext,air}$ = 915 s^{-1}). At ϕ = 0.60, the maximum temperature of the oxy-flame increases at lower strain rate as shown in Figure 14; however, at ϕ = 0.67, the maximum temperature does not increase, and starts to decrease earlier than that of an air-flame. In previous PIV measurements [9], within the mean boundaries

of the inner recirculation zone, the flame strain distribution is entirely below the extinction limit and hence flames are always observed along the inner shear layer. However, the local strain rate is found to be around 3000 1/s or more in the outer shear layer at $\phi = 0.60$. This is beyond the extinction strain rate at this ϕ and if persistent could imply absence of flames in the outer shear layer. Turbulent flames, however, do not experience a steady strain. If the strain rate fluctuates, flames do not immediately extinguish when the static extinction limit is reached. Egolfopoulos examined the mechanism of unsteady extinction in laminar premixed flames, and found that for sufficiently high frequency oscillations, extinction may be delayed or suppressed [17]. Thus, average strains higher than the static extinction value may not always lead to flame extinction. On the other hand flames in the outer shear layers may also be weakened by heat loss to the walls. Therefore, a possible explanation for the absence of an air flame there, and for oxy-flames stabilization in the outer shear layer is their resistance to extinction at higher strain rate even in the presence of heat loss (this will be shown in future calculations). We should add that the laminar burning velocity and strained flame speed are both higher for the air flame, and hence they do not offer a reason for the persistence of the oxy-flame and extinction of the air flames in the outer shear layer. Only the better resistance of the oxy-flame to strain is consistent with the experimental results. In the following we examine the flame structure further to explain oxy-flame resistance to extinction.

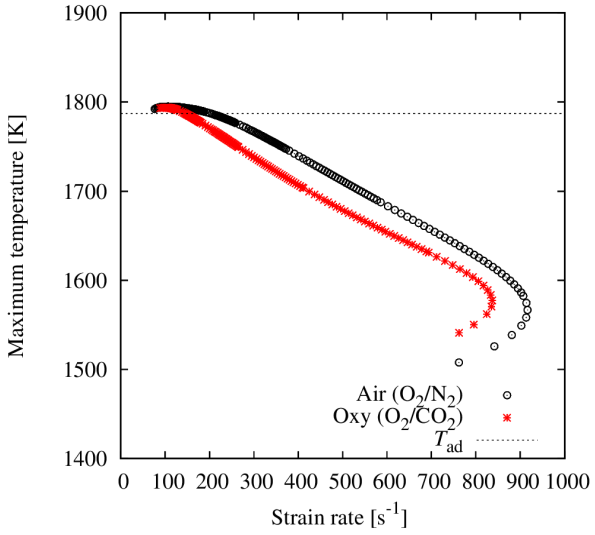

Figure 15 : Response of maximum temperature to the strain rate at $\phi = 0.67$

Flame extinction calculation (Profiles)

In the counter flow configuration, with increasing the strain rate, the reaction zone reaches the stagnation plane, and the flame thickness decreases while approaching the turning point (extinction point).

Figure 16 shows profiles of temperature, and OH, H, and CH radical concentrations of twin premixed air and oxy-flames at k = 490 s^{-1} at (a) ϕ = 0.60 and (b) ϕ = 0.67. Profiles at specific strain rate (k = 490 s^{-1}) are shown here since radical concentration profiles show similar trends at various strain rate.

First, at $\phi = 0.60$, OH radical concentrations of oxy-flames are higher than those of air flames. Inlet O_2 concentrations of oxy-flames are higher than that of air-flames. Higher O_2 concentration produces more OH and O radicals through the main chain branching reaction:

$$O_2 + H \rightarrow OH + O \qquad (R1)$$

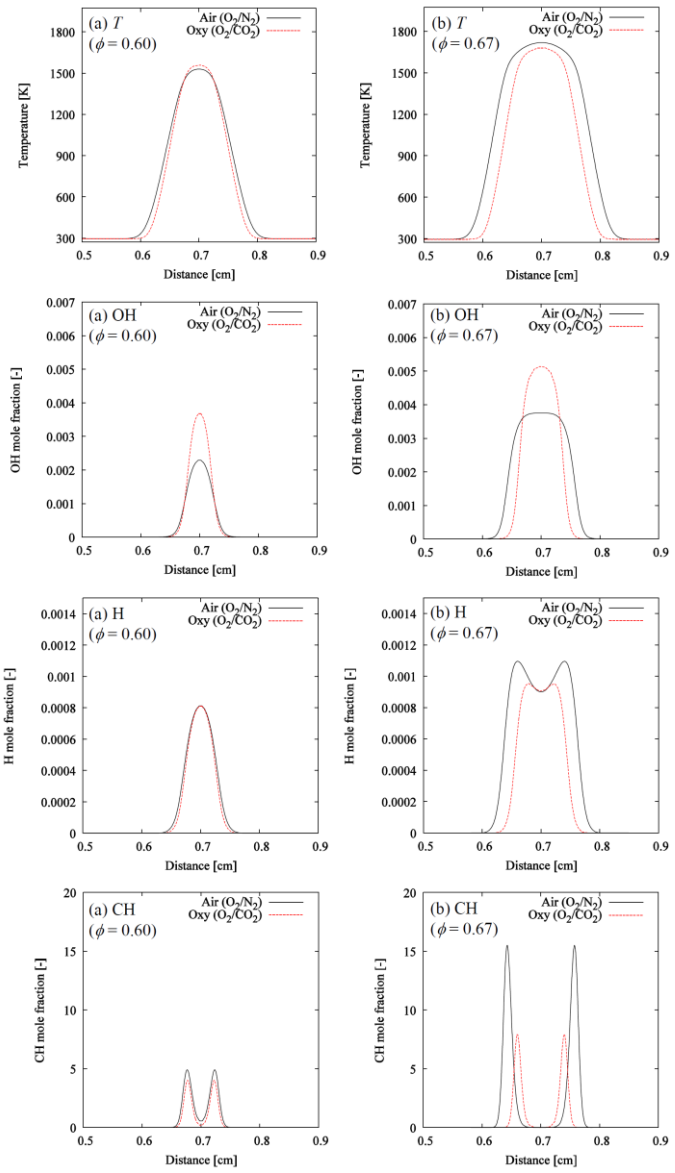

Figure 16: Calculated profiles of temperature, OH, H, and CH of twin premixed air and oxy-flames at 490 s^{-1} (a) ϕ = 0.60 and (b) ϕ = 0.67

R1 is the most important reaction in OH radical production. Meanwhile, insignificant difference between air and oxy-flames is found in the H profiles, and CH profiles of oxy-flames are slightly lower than that of air-flames at $\phi = 0.60$.

On the other hand, significant difference between air and oxy-flames is observed in radical profiles at $\phi = 0.67$. Similar to $\phi = 0.60$, OH radical concentrations in an oxy-flame are higher than those in an air flame. However, H and CH radical concentrations in oxy-flame are lower than those in air-flame. Reaction analyses show that the following reaction rate increases with increasing the equivalence ratio, resulting in lower H radicals.

$$CO_2 + H \rightarrow CO + OH \qquad \text{(R2)}$$

Many researchers have shown that high levels of CO_2 reduce the H radical through the R2, leading to lower concentration of chain carriers via R1 [18,19]. Due to the competitive reactions for H radicals, the rate of CH_4 oxidation in oxy-flames is lower than that in air flame under fuel-lean conditions. Therefore, CH radical concentration in oxy-flames is lower than in air-flames at $\phi = 0.67$. Meanwhile, with decreasing the equivalence ratio, the H radical concentration decreases, and the competitive reaction for H radicals becomes less important. This is the reason why the difference of H and CH radical concentrations is insignificant at $\phi = 0.60$. When radical concentrations are similar in both air and oxy-flames, the effect of CO_2 transport properties becomes important in the flame stabilities, leading to appearance of the cross point. The details will be discussed next.

Flame consumption speed

The consumption speed S_c of the flame is defined as:

$$S_c = \frac{\int_{-\infty}^{\infty} q'''/c_p \, dx}{\rho_u (T_b - T_u)} \qquad (4)$$

where q''' is the volumetric heat release rate, c_p is the specific heat of the mixture, x is the axial coordinate, ρ_u is the unburned mixture density, and T_u and T_b are the unburned and burned temperature, respectively. In this section, additional oxy-flame calculation using CO_2 with N_2 transport properties (defined as oxy*) is performed. By changing transport properties of CO_2 to those of N_2 in the oxy* calculation, the effect of transport properties on flame stability is revealed. In the oxy* calculation, the specific heat (C_p) and density (ρ) are set to CO_2 properties to keep the same temperature, whereas diffusion coefficient (D_i), thermal conductivity (λ) and viscosity (μ) are set to N_2 properties.

Figure 17 and Figure 18 show the flame consumption speed for air, oxy-flames, and oxy*-flames near the extinction strain at $\phi = 0.60$ and 0.67, respectively. Flame extinction occurs at the turning point of the flame consumption speed. At $\phi = 0.60$, extinction strain rate of oxy-flames is higher than that of air-flames, whereas that of oxy*-flames is lower than that of air-flames. In fact, the CO_2 transport properties improve the stability of flame, resulting in higher extinction strain rate at $\phi = 0.60$. However, with increasing the equivalence ratio, the competitive reaction for H radicals between R1 and R2 becomes important as mentioned in the previous section. Therefore, the extinction strain rates of oxy-flames are lower than those of air-flames at $\phi = 0.67$, even though the CO_2 transport properties increase the extinction strain rate.

Transport properties and chemical reactivities influence the extinction strain rate. Lower diffusion in CO_2 environments increases the extinction strain rate, whereas CO_2 reactivity expressed in R2 reduces the extinction strain rate through the competitive reactions for H radicals. Therefore, while $\varepsilon_{ext,oxy} > \varepsilon_{ext,air}$ at $\phi = 0.60$, it reverses at $\phi = 0.67$.

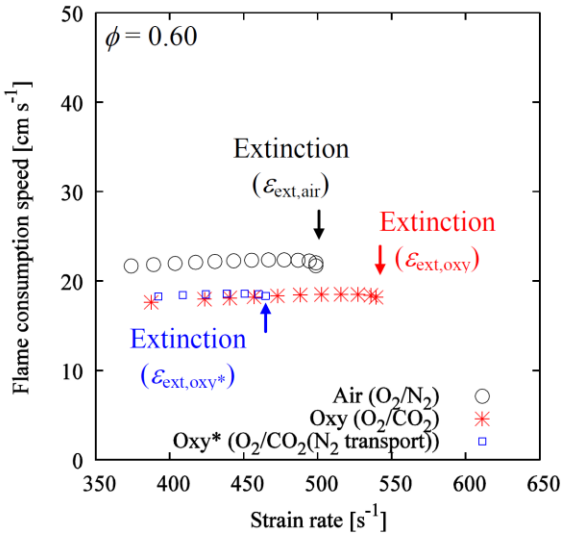

Figure 17: Flame consumption speed for air and oxy-flames near extinction strain rate at $\phi = 0.60$

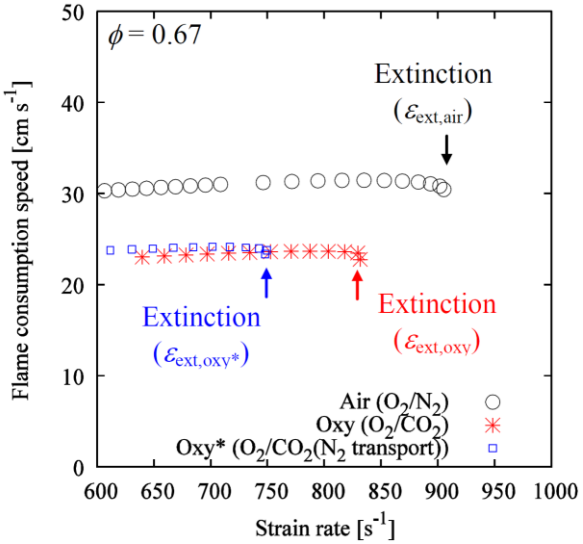

Figure 18: Flame consumption speed for air and oxy-flames near extinction strain rate at $\phi = 0.67$

CONCLUSION

In this study, premixed $CH_4/O_2/CO_2$ flames (oxy-flames) and CH_4/air flames (air-flames) were experimentally studied in a swirl-stabilized combustor. For comparing oxy and air flames, the same equivalence ratio and adiabatic flame temperature were used. In order to explain some of the observations, the extinction strain in both flames was obtained using the twin-flame configuration. Overall, in both cases, as the equivalence ratio is reduced, the flame length becomes longer. Notable differences between the two flames appear as the equivalence ratio reaches 0.60, when the outer shear layer flame disappears in the air-flames while it persists in the oxy-flame. Prior PIV experiments (Ref. 9) showed that the strains along the outer shear layer are mostly higher than along the inner shear layer. Premixed twin flame calculations at this equivalence ratio show that the extinction strain rate is higher in the oxy than in the air flame, which may help explain why oxy-flames persist on the outer shear layer with higher strain rate. It is likely that extinction strain rates are one of the mechanisms responsible for oxy-flame stabilization on the outer shear layer when the air flame extinguish. The CO_2 transport properties increase extinction strain rate of oxy-flames. However, with increasing the equivalence ratio, the extinction strain of oxy flames is found to be lower under these conditions because the competition for H radicals between $O_2 + H \rightarrow OH + O$ (R1) and $CO_2 + H \rightarrow CO + OH$ (R2) becomes important, and the cross point of the extinction strain appears at equivalence ratio of 0.64. Our analysis so far shows that the higher resistance of the oxy-flame at relatively lower equivalence ratio can be used to explain the experimental observation.

ACKNOWLEDGMENTS

This work was supported by a grant from King Abdullah University of Science and Technology (KAUST), Grant No. KUS-110-010-01.

REFERENCES

[1] Kvamsdal, H., Jordal, K., Bolland, O., 2007, "A Quantitative Comparison of Gas Turbine Cycles with CO_2 capture," *Energy, Vol. 32*, pp. 10-24.

[2] Liu, H., Okazaki, K., 2003, "Simultaneous easy CO_2 recovery and drastic reduction of SO_x and NO_x in O_2/CO_2 coal combustion with heat recirculation," *Fuel*, Vol. 82, pp. 1427-1436.

[3] Watanabe, H., Yamamoto, J., Okazaki, K., 2011, "NO_x formation and reduction mechanisms in staged O_2/CO_2 combustion," *Combust. Flame*, Vol. 158, pp. 1255-1263.

[4] Kobayashi, H., Hagiwara, H., Kaneko, H., Ogami, Y., 2007, "Effects of CO_2 dilution on turbulent premixed flames at high pressure and high temperature," *Proc. Combust. Inst.*, *Vol. 31*, pp. 1451-1458.

[5] Maruta, K., Law, C. K., Takeno, T., 1996, "A Flame-Controlling Continuation Method for Generating S-Curve Responses with Detailed Chemistry," *Combust. Flame, Vol. 104*, pp. 328-342.

[6] Shroll, A. P., Shanbhogue, S. J., Ghoniem, A. F., 2012, "Dynamic-Stability Characteristics of Premixed Methane Oxy-Combustion," *J. Eng. Gas Turbines Power*, *Vol. 134*, 051504.

[7] Taamallah, S., LaBry, Z., Shanbhogue, S. J. and Ghoniem, A. F., 2014, "Correspondence Between Uncoupled Flame Macrostructures and Thermoacoustic Instability in Premixed Swirl-Stabilized Combustion," *J. Eng. Gas Turbines Power, accepted for publication*.

[8] Taamallah, S., LaBry, Z., Shanbhogue, S. J. and Ghoniem, A. F., 2014, "Thermo-acoustic instabilities in lean premixed swirl-stabilized combustion and their link to acoustically coupled and decoupled flame macrostructures," *Proc. Combust. Inst., (in press).*

[9] LaBry, Z., Kewlani, G., Taamallah, S., Shanbhogue, S. J. and Ghoniem, A. F., 2014, "Mode transition and intermittency in an acoustically uncoupled lean premixed swirl-stabilized combustor," *Proceedings of ASME Turbo Expo 2014*, GT2014-27266.

[10] LaBry, Z. A., 2014, "Turbulent Flame Microstructure, Dynamics, and Thermoacoustic Instability in Swirl-Stabilized Premixed Combustion: Measurements, Statstics and Analysis," Ph.D. Thesis, Massachusetts Institute of Technology, Cambridge, MA.

[11] Thumuluru, S. K., Lieuwen, T., 2009, "Characterization of acoustically forced swirl flame dynamics," *Proc. Combust. Inst.*, Vol. 32, pp. 2893-2900.

[12] Bellows, B. D., Bobba, M. K., Forte, A., Seitzman, J. M., Lieuwen, T., 2007, "Flame transfer function saturation mechanisms in a swirl-stabilized combustor," *Proc. Combust. Inst., Vol. 31*, pp. 3181-3188.

[13] Bulat, G., Fedina, E., Fureby, C., Meier, W., Stopper, U., 2014, "Reacting flow in an industrial gas turbine combustor: LES and experimental analysis," *Proc. Combust. Inst., (in press).*

[14] Mendiara, T., Glaborg, P., 2009, "Ammonia chemistry in oxy-fuel combustion of methane," *Combust. Flame, Vol. 156*, pp. 1937-1949.

[15] Taamallah, S., Shanbhogue, S., Sanusi, Y., Mokhiemer, E. and Ghonime, A.F., Transition from a single to a double flame structure in a swirling reacting flow: mechanism, dynamcis and effect of thermal boundary condition, Proc of ASME Turbo Expo, GT2015, June 15-19, 2015, Montreal, CA, GT2015-43998.

[16] Law, C. K., 1988, "Dynamics of stretched flames," *Twenty-Second Symp. (Int.) Combust*., pp. 1381-1402.

[17] Egolfopoulos, F. N., 1994, "Dynamics and structure of unsteady, strained, laminar premixed flames," 1994, *Twenty-Fifth Symp. (Int.) on Combust*., pp. 1365-1373.

[18] Cong, T. L., Dagaut, P., 2009, *Proc. Combust. Inst. Vol. 32*, pp. 427–435.

[19] Abián, M., Giménez-López, J., Bilbao, R., Alzueta, M. U., 2011, *Proc. Combust. Inst., Vol. 33*, pp. 317–323.